Supporting information:

# High-performance silicon photoanode enhanced by gold nanoparticles for efficient water oxidation

*Wenting Hong*[†‡], *Qian Cai*[†], *Rongcheng Ban*[⊥], *Xu He*[†], *Chuanyong Jian*[†], *Jing Li*[†], *Jing Li*[⊥], *Wei Liu*[*†]

[†]CAS Key Laboratory of Design and Assembly of Functional Nanostructures, and Fujian Provincial Key Laboratory of Nanomaterials, Fujian Institute of Research on the Structure of Matter, Chinese Academy of Sciences, Fuzhou, Fujian, 350002, China

[‡]University of Chinese Academy of Sciences, Beijing, 100049, China

[⊥]Department of Physics/Pen-Tung Sah Institute of Micro-Nano Science and Technology, Xiamen University, Xiamen, Fujian 361005, China

E-mail: liuw@fjirsm.ac.cn

**S1. The height of the surface of NiAu/$TiO_2$/n-Si photoanode with NiAu (2 nm/2 nm) catalyst**

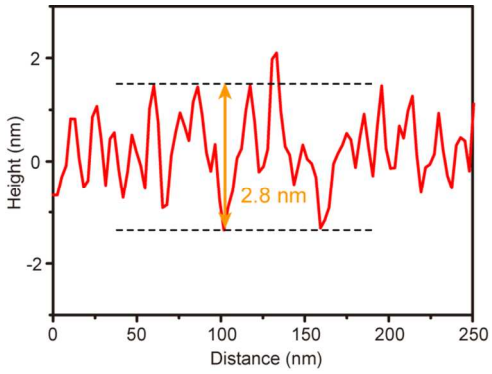


**Figure S1.** The corresponding height profile of the white line in Atomic force microscopy (AFM) image (figure 1c).

**S2. The possible deposited process of NiAu catalyst**

The structures of as-prepared samples are determined by X-ray photoelectron spectroscopy (XPS) using Ar Kα radiation (ESCALAB 250Xi). The depth profile of Au 4f and Ni 2p signals are collected at various etch times using Ar ion milling method.

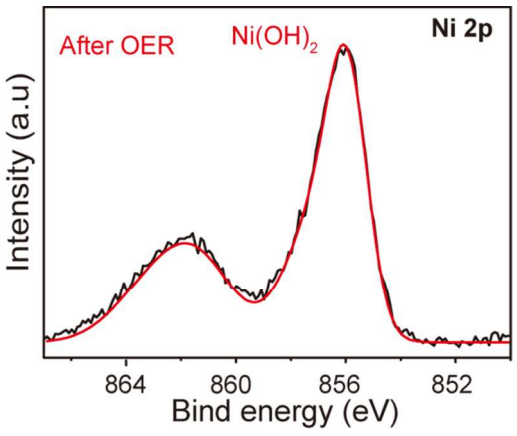


**Figure S2.** X-ray photoelectron spectroscopy (XPS) spectra of Ni 2p spectra for NiAu/$TiO_2$/n-Si photoanode after OER operation.

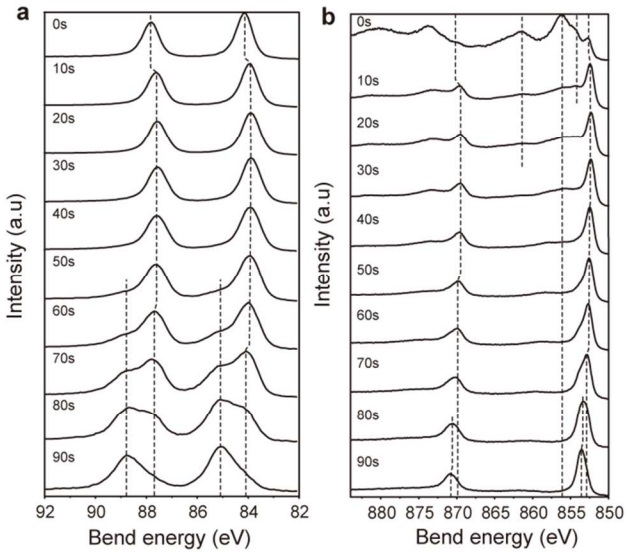


**Figure S3.** The depth profiling of a, Au, b, Ni for NiAu catalyst under different etching times.

**S3. Photoelectrochemical characterization methods**

In this study, all electrochemical reactions were measured using Ag/AgCl reference electrode at room temperature. However, all the measurements discussed are performed in 1M KOH solution electrolyte of pH = 14 using Pt counter electrode and converted to the reversible hydrogen electrode (RHE) unless specified. The converting equation is $E_{RHE} = E_{SCE} + 0.197\ V + 0.059*pH$, where $E_{RHE}$ is the potential referred to RHE and $E_{SCE}$ is the measured potential against saturated calomel electrode (SCE) electrode filled with 3.5 M KCl as the reference electrode. All the current density values given in the text refer to the visible area of the working electrode (1.0 $cm^2$). The onset potential, defined as the potential to drive the current density of 1 $mA/cm^2$ for water oxidation, and the photocurrent density at 1.23 V versus RHE are the criterions in this work to evaluate the OER activity. They can be obtained from LSV curves. All data are collected without iR compensation. The OER testing is operated under visible light irradiation, and a UV-cutoff filter was employed to achieve visible-light (>420 nm) irradiation.

The photovoltage was defined as the difference between the potential to drive 1 mA/cm$^2$ through the illuminated n-Si photoanode and the dark $p^+$-Si anode. The NiAu/$TiO_2$/n-Si photoanode has a high photovoltage around 518 mV as shown in Figure S4 a.

Electrochemical impedance spectroscopy was performed in 1M KOM solution in dark, the AC voltage was 5 mV amplitude with the frequency range from 0.1 Hz to 10000 Hz. The initial potential is around their corresponding onset potential.

**Table S1** OER catalytic parameters of recently-reported Ni-based and Si-based photoanodes.

| Photoanodes | $\eta_0$ (V) | $J_{sc}$ (mA/cm$^2$) | Electrolyte | Reference |
|---|---|---|---|---|
| **NiAu (2nm/2 nm)/$TiO_2$/n-Si** | **-0.20** | **18.80** | **1M KOH** | **This work** |
| **Ni (2 nm)/$TiO_2$/n-Si** | **-0.13** | **8.62** | **1M KOH** | **This work** |
| $Ni_{80}Fe_{20}$/$TiO_2$/n-Si | -0.17 | 21.5 | 1M KOH | *ACS Catal.* 2017, *7*, 3277-3283.[1] |
| np+-Si\|$NiO_x$ | -0.18 | 29 | 1M KOH | *J. Phys. Chem. Lett.* 2015, *6*, 592-598.[S1] |
| np + -Si/$SiO_x$/NiFe | -0.34 | 30.7 | 1M KOH | *Adv. Energy Mater.* 2016, *7*, 1601805.[S2] |
| 2 nm Ni/2 nm Ti/n-Si | -0.20 | 10.7 | 1 M KOH | *J. Mater. Chem. A* 2017, *5*, 1996-2003.[S3] |
| 5 nm Ni/$SiO_X$/n-Si | -0.078 | 0.8 | 1 M KOH | *J. Mater. Chem. A* 2016, *4*, 8053-8060.[28] |
| Ni NP/$SiO_X$/n-Si | -0.16 | 3.5 | 1 M NaOH | *ACS Energ. Lett.* 2017, *2*, 569-573.[29] |
| n-Si/$TiO_2$/Ni | -0.03 | 1.8 | 1 M KOH | *ACS Appl. Mater. Interfaces* 2015, *7*, 15189-15199.[30] |
| $NiMoO_4$/$TiO_2$/Si nanowire | 0.85 | 0.014 | 1 M KOH | *Nano Energ.* 2017, *34*, 8-14.[S4] |
| n-Si/$SiO_{x,RCA}$/$CoO_x$ | -0.212 | 23.2 | 1 M KOH | *Energy Environ. Sci.* 2016, *9*, 892-897.[31] |
| n-Si/$NiO_x$ | 0.13 | 0.2 | 0.25M $Na_2SO_4$ | *Energy Environ. Sci.* 2012, *5*, 7872-7877.[14] |
| $CoO_x$/ $SiO_x$/ $np^+$Si | -0.13 | 17 | 1 M NaOH | *J. Am. Chem. Soc.* 2014, *136*, 6191-6194.[S5] |
| Ni/$SiO_x$/ n-Si | -0.16 | 10.47 | 1 M KOH | *Science* 2013, *342*, 836-840.[16] |
| Ni/$TiO_2$/ $np^+$-Si | -0.16 | 11 | 1 M KOH | *Science* 2014, *344*, 1005-1009.[17] |
| $IrO_x$/Ir/$p^+$-n-Si | -0.18 | 13.8 | 1 M $H_2SO_4$ | *J. Phys. Chem. Lett.* 2014, *5*, 3456-3461.[S6] |
| n-Si\|$SiO_x$\|$TiO_2$\|Ir | -0.21 | 8.34 | 1 M NaOH | *Nat. Mater.* 2015, *15*, 99-105.[8] |
| $Fe_2O_3$/n-SiNW | -0.23 | 17.3 | 1M NaOH | *Angew. Chem. Int. Ed.* 2012, *51*, 423-427.[S7] |
| n-Si/$SiO_x$ /$CoO_x$/$NiO_x$ | -0.24 | 27.7 | 1 M KOH | *Energy Environ. Sci*. 2015, *8*, 2644-2649.[S8] |
| $NiRuO_x$/ n-bSi | -0.25 | 1.34 | 0.25M $Na_2SO_4$ | *Nano Lett.* 2013, *13*, 2064-2072.[S9] |
| Ir/$TiO_2$/$SiO_2$/$p^+$n-Si | -0.3 | 4.8 | PBS | *Nat. Mater.* 2011, *10*, 539-544.[12] |
| $Ni(OH)_2$-Au | 0.12 | / | 1 M KOH | *J. Am. Chem. Soc.* 2016, *135*, 16977-16987.[35] |
| AuNP/Hematite/SiNW | -1.25 | 2.6 | 1M NaOH | *Nano Lett*. 2014, *14*, 18-23.[19] |

$\eta_0$: water oxidation overpotential at 1 mA/cm$^2$ current density; $J_{sc}$: the photocurrent density at 1.23 V versus RHE.

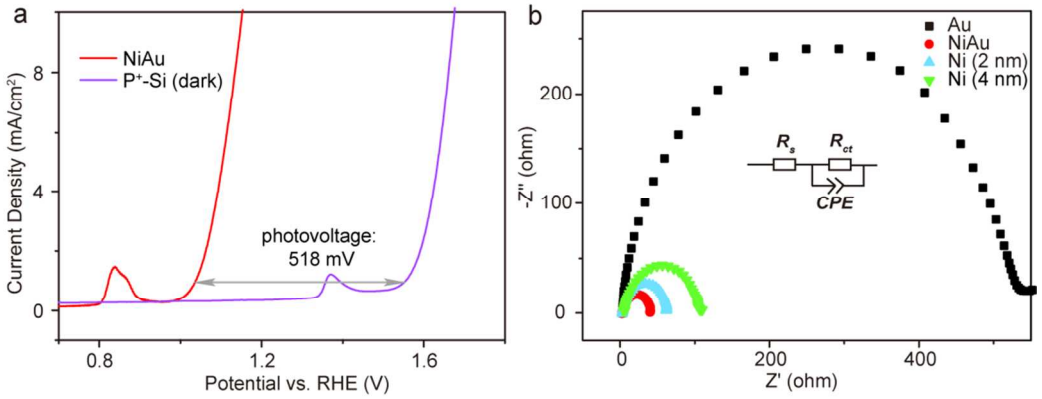


**Figure S4** a, LSV curves for NiAu/$TiO_2$/n-Si and NiAu/$TiO_2$/$p^+$-Si photoanodes. b, Nyquist diagrams for various metal/$TiO_2$/n-Si photoanodes, the inset shows the equivalent circuit model.

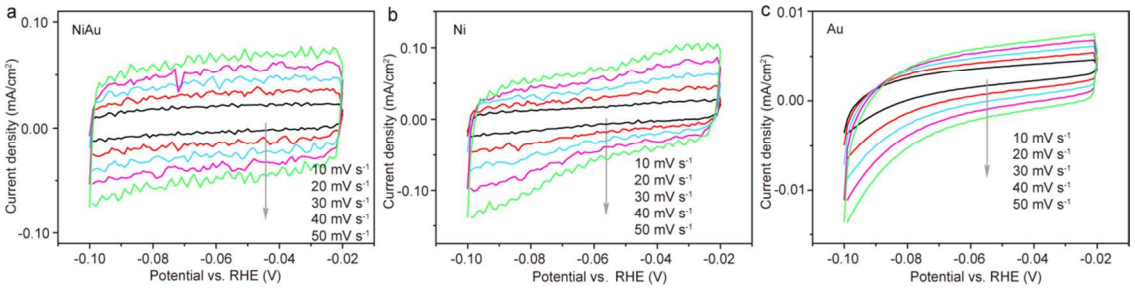


**Figure S5.** Electrochemical cyclic voltammetry curves of a, NiAu/$TiO_2$/n-Si, b, Ni/$TiO_2$/n-Si and c, Au/$TiO_2$/n-Si photoanodes at different scanning rates.

**S4. FDTD solutions method**

A UV-VIS (NIR) Spectrophotometer (Lambda950) was used to record optical transmission spectra of the Au nanoparticles. Finite-difference-time-domain (FDTD) was also used to simulate the UV-visible absorbance. The dimensions for FDTD calculation are extracted from the AFM image (Figure 1c).

For simplicity, the Au and Ni nanoparticles were considered as nanospheres, where the diameter was 2 nm. Au nanoparticles (yellow) were distributed on the 2 nm $TiO_2$ film and 100 nm n-Si wafer, while Ni nanoparticles (green) were embedded on the interspace of the Au

nanoparticles (yellow). To get the precise optical characteristics, the grid was set to 0.05 nm and the simulation time as 1000 fs. The optical constants of Si, Au, Ni, and $TiO_2$ were taken from Palik.[S10] A 546 nm plane wave light with normal incident was used to simulate the spatial distribution of plasmonic field for NiAu/$TiO_2$/n-Si photoanode (Figure 5a), as shown in figure S6. The simulation area was marked by the red dashed line frame.

The simulation for UV-visible absorbance spectra in Figure 3d was of the same parameters, besides the absence of n-Si substrate and $TiO_2$ layer. Only NiAu catalyst was modeled to study the absorption since the absorption of n-Si substrate was used to be the base line in the measured absorbance spectra and $TiO_2$ layer had a negligible impact on absorption with the wavelength larger than 440 nm.

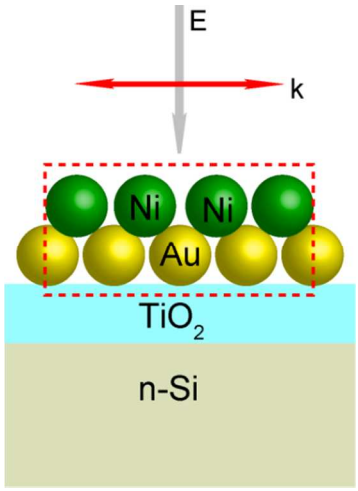


**Figure S6.** The calculation models of Au and Ni nanoparticles complex arrays employed in the simulation by the finite-difference-time-domain (FDTD) solutions.

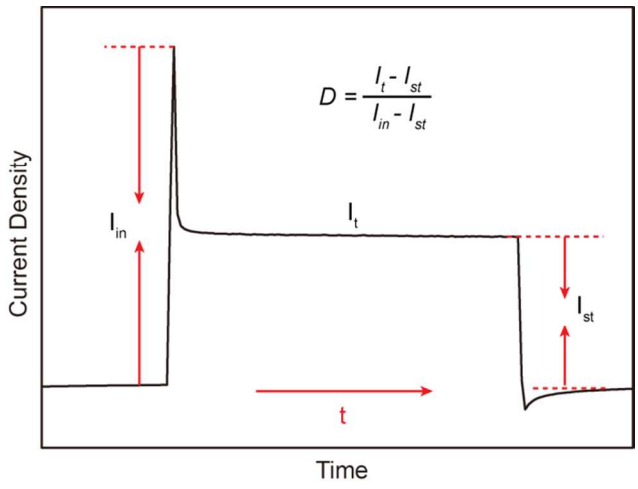


**Figure S7.** The scheme for the calculation of the transient dynamics is constant, the inset shows the equation of the normalized parameter (*D*).

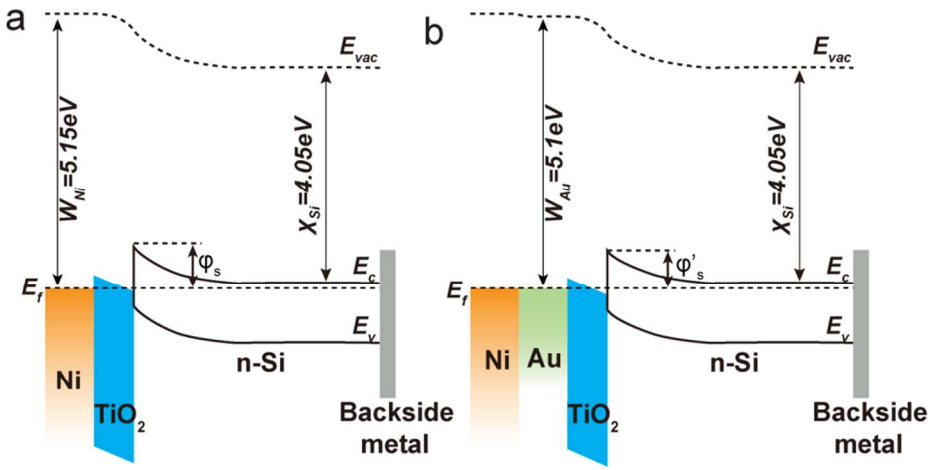


**Figure S8.** Approximate energy band diagram with respect to the vacuum level of a), Ni/$TiO_2$/n-Si structure and b), NiAu/$TiO_2$/n-Si structure.

REFERENCES

**References**

(S1) Sun, K.; McDowell, M. T.; Nielander, A. C.; Hu, S.; Shaner, M. R.; Yang, F.; Brunschwig, B. S.; Lewis, N. S. Stable Solar-Driven Water Oxidation to $O_2$ (g) by Ni-Oxide-Coated Silicon Photoanodes. *J. Phys. Chem. Lett.* **2015**, *6*, 592-598.

(S2) Yu, X.; Yang, P.; Chen, S.; Zhang, M.; Shi, G. NiFe Alloy Protected Silicon Photoanode for Efficient Water Splitting. *Adv. Energy Mater.* **2017**, *7*, 1601805.

(S3) Shi, Y.; Han, T.; Gimbert-Suriñach, C.; Song, X.; Lanza, M.; Llobet, A. Substitution of Native Silicon Oxide by Titanium in Ni-Coated Silicon Photoanodes for Water Splitting Solar Cells. *J. Mater. Chem. A* **2017**, *5*, 1996-2003.

(S4) Wu, F.; Liao, Q.; Cao, F.; Li, L.; Zhang, Y. Non-Noble Bimetallic $NiMoO_4$ Nanosheets Integrated Si Photoanodes for Highly Efficient and Stable Solar Water Splitting. *Nano. Energy* **2017**, *34*, 8-14.

(S5) Yang, J.; Walczak, K.; Anzenberg, E.; Toma, F. M.; Yuan, G.; Beeman, J.; Schwartzberg, A.; Lin, Y. J.; Hettick, M.; Javey, A.; Ager, J. W.; Yano, J.; Frei, H.; Sharp, I. D. Efficient and Sustained Photoelectrochemical Water Oxidation by Cobalt Oxide/Silicon Photoanodes with Nanotextured Interfaces. *J. Am. Chem. Soc.* **2014**, *136*, 6191-6194.

(S6) Mei, B.; Permyakova, A. A.; Frydendal, R.; Bae, D.; Pedersen, T.; Malacrida, P.; Hansen, O.; Stephens, I. E. L.; Vesborg, P. C. K.; Seger, B.; Chorkendorff, I. Iron-Treated NiO as a Highly Transparent p-Type Protection Payer for Efficient Si-Based Photoanodes. *J. Phys. Chem. Lett.* **2014**, *5*, 3456-3461.

(S7) Jun, K.; Lee, Y. S.; Buonassisi, T.; Jacobson, J. M. High Photocurrent in Silicon Photoanodes Catalyzed by Iron Oxide Thin Films for Water Oxidation. *Angew. Chemie. Int. Ed.* **2012**, *51*, 423-427.

(S8) Zhou, X.; Liu, R.; Sun, K.; Friedrich, D.; McDowell, M. T.; Yang, F.; Omelchenko, S. T.; Saadi, F. H.; Nielander, A. C.; Yalamanchili, S.; Papadantonakis, K. M.; Brunschwig, B. S.; Lewis, N. S. Interface Engineering of the Photoelectrochemical Performance of Ni-Oxide-Coated n-Si Photoanodes by Atomic-Layer Deposition of Ultrathin Films of Cobalt Oxide. *Energy Enviro. Sci.* **2015**, *8*, 2644-2649.

(S9) Sun, K.; Pang, X.; Shen, S.; Qian, X.; Cheung, J. S.; Wang, D. Metal Oxide Composite Enabled Nanotextured Si Photoanode for Efficient Solar Driven Water Oxidation. *Nano Lett.* **2013**, *13*, 2064-2072.

(S10) Palik, E. D. *Handbook of Optical Constants of Solids.* Academic press, New York, 1985.